Bulletin of Mathematical Biology Vol. 55, No. 3, pp. 637–654, 1993.
Printed in Great Britain.

0092–8240/93$6.00+0.00
Pergamon Press Ltd

STRESS-INDUCED ALIGNMENT OF ACTIN FILAMENTS AND THE MECHANICS OF CYTOGEL

■ JONATHAN A. SHERRATT
Centre for Mathematical Biology,
Mathematical Institute,
24–29 St Giles',
Oxford OX1 3LB, U.K.

Email:jas@vax.oxford.ac.uk

■ JULIAN LEWIS
ICRF Developmental Biology Unit,
Department of Zoology,
University of Oxford,
South Parks Road,
Oxford OX1 3PS, U.K.

Experimental evidence suggests that anisotropic stress induces alignment of intracellular actin filaments. We develop a model for this phenomenon, which includes a parameter reflecting the sensitivity of the microfilament network to changes in the stress field. When applied to a uniform cell sheet at rest, the model predicts that for sufficiently large values of the sensitivity parameter, all the actin filaments will spontaneously align in a single direction. Stress alignment can also be caused by a change in external conditions, and as an example of this we apply our model to the initial response of embryonic epidermis to wounding. Our solutions in this case are able to reflect the actin cable that has been found at the wound edge in recent experiments; the cable consists of microfilaments aligned with stress at the wound boundary of the epithelium. These applications suggest that stress-induced alignment of actin filaments could play a key role in some biological systems. This is the first attempt to include the alignment phenomenon in a mechanical model of cytogel.

1. Biological background. The mechanical balance of forces in living tissue has formed the basis for many recent models of developmental morphogenesis. This approach was introduced by Odell *et al.* (1981), who developed a discrete model for the folding of embryonic epithelia. Building on this work, G. F. Oster, J. D. Murray and their colleagues (Oster *et al.*, 1983; Murray *et al.*, 1983; Murray and Oster, 1984a,b; Oster *et al.*, 1985a,b; Murray *et al.*, 1988) developed a series of continuum mechanochemical models for pattern formation in a wide range of embryonic systems. In the Oster–Murray approach, cytogel is treated as an isotropic viscoelastic continuum, and the non-viscous response to applied strain is the same as for, say, a simple rubber sheet, except for the exertion of an isotropic contraction stress. Experimentally,

such traction forces have been observed in a number of cell types (see Harris, 1982; and refs in Stopak *et al.*, 1985). In the model equations, this traction stress is analogous to a "negative pressure", and is crucial to the predictions of the various models.

In reality, of course, there are other differences between the non-viscous response to applied strain of simple non-living materials, such as a rubber sheet, and of cytogel. In this paper, we focus on one such difference, namely the alignment of actin filaments with the stress field, which is illustrated schematically in Fig. 1. Intracellular actin filaments determine many of the mechanical properties of a confluent cell sheet (Pollard, 1990), and the alignment phenomenon has been recognized but neglected in previous applications of the Oster–Murray approach (for example, Oster and Odell, 1984a). Here we develop a new model which reflects stress alignment, and discuss two simple applications, which highlight the importance of the phenomenon in some biological systems.

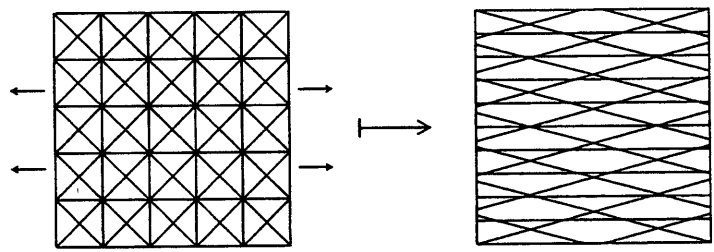

Figure 1. A diagrammatic representation of stress-induced actin filament alignment. The filaments tend to align with the applied stress field.

We begin by briefly reviewing the experimental evidence for stress-induced alignment of actin filaments. The seminal work is by Kolega (1986). He studied the cytoskeleton of fish epidermal cells held under tension either by micromanipulation or by cellular locomotive activity, and found that the actin filaments were aligned parallel to the tension. Moreover, in the case of micromanipulation, filament alignment occurred within a few minutes, as a direct response to applied tension.

Although not as clear as Kolega's (1986) study, previous authors had found a similar response to applied tension. Chen (1981) investigated the retraction of fibroblast tails following detachment from the substratum. In common with previous authors (for example Spooner *et al.*, 1971; Ludueña and Wessells, 1973) he found that a taut elongated tail contained bundles of microfilaments extending parallel to the long axis, and thus aligned with the stress field. Upon detachment, these microfilament bundles lost their orientation and returned to a random mesh-like arrangement; this conversion took about 15 sec. Valberg

and Albertini (1985) used a magnetic particle method to study the effects of applied tension on pulmonary macrophages from the lungs of hamsters. They caused the macrophages to ingest magnetic particles, which then entered phagosome organelles, and they applied external magnetic fields. This resulted in positive staining for actin coinciding with the location of the magnetic particles, which again suggests stress-induced microfilament alignment. Finally, a number of authors have studied the alignment of actin filament bundles in endothelial cells under shear stress. This is an important feature of blood flow, and occurs in both isolated cells and in confluent cell sheets (see, for example, Franke *et al.*, 1984; Wechezak *et al.*, 1989).

2. A Model for Filament Alignment. The detailed biological mechanisms by which an applied stress field induces actin filament alignment are largely unknown. We therefore base our model on simple, intuitively plausible assumptions. Most importantly, we assume that alignment occurs as a direct response to the ratio of the principal components of stress. This implies that multiplying the stress tensor by an isotropic factor will have no effect on the actin filament network; in reality, there may be an increase in the proportion of actin that is polymerized (Pender and McCulloch, 1991), but here for simplicity we take any such increase to be negligible. We will denote the principal axes of the stress tensor $\underline{\underline{\sigma}}$ as the 1- and 2-axes, with corresponding principal values σ_1 and σ_2. These axes are orthogonal since $\underline{\underline{\sigma}}$ will always be symmetric. With this notation, we represent the microfilament network via the density function $F(\phi; \rho)$, defined by the condition that $F(\phi; \rho)\delta\phi$ is the continuum average of the proportion of the actin filaments inclined to the 1-axis at angles in the range $(\phi, \phi+\delta\phi)$, when $\sigma_1/\sigma_2 = \rho$. Thus F is also a function of space, but since all our calculations will be at a single point in space, we do not include $\underline{r}$ as an argument of F, for notational simplicity. The symmetries of the system are such that $F(-\phi, \rho)$ and $F(\phi+\pi, \rho)$ must both equal $F(\phi, \rho)$, and we can therefore restrict our attention to values of ϕ in $[0, \pi/2]$. We require F to satisfy the following conditions.

(a) $F(\phi; \rho) \to \delta(\pi/2-\phi)$ as $\rho \to 0$ and $F(\phi; \rho) \to \delta(\phi)$ as $\rho \to \infty$, where δ denotes the Dirac delta function. That is, when the stress field is unidirectional, all filaments are oriented in that direction.

(b) $\int_0^{\pi/2} F(\phi; \rho)\, d\phi = 1$, since F is a density function. Thus the total number of microfilaments is unchanged by the process of stress alignment: as discussed above, we assume that changes in the stress field do not affect the extent of actin polymerization.

(c) $F(\phi; 1)$ is a constant. That is, when the stress field is isotropic the filaments are oriented randomly. Condition (b) implies that the value of this constant is $2/\pi$.

(d) $F(\phi;\rho)=F(\pi/2-\phi;1/\rho)$, by symmetry.

These conditions do not determine F, but they are fairly restrictive. In particular, the definition of the Dirac delta function as $\delta(x)=\lim_{\varepsilon\to 0}(1/\varepsilon\sqrt{\pi})\exp[-x^2/\varepsilon^2]$ suggests the following functional form:

$$F(\phi;\rho)=F_0(\rho)\left[\frac{1}{\psi(\rho)}\exp\left\{-\frac{k(\pi/2-\phi)^2}{\psi(\rho)^2}\right\}+\psi(\rho)\exp\{-k\psi(\rho)^2\phi^2\}\right] \quad (1)$$

where k is a positive constant and $\psi(0)=0$, $\psi(1)=1$ and $\psi(\infty)=\infty$. We choose $F_0(\rho)$ such that condition (b) is satisfied. If we take $\psi(\rho)=\rho^p$ for some $p>0$ then condition (d) is also satisfied.

It remains to consider condition (c), that $F(\phi;1)$ is independent of ϕ. This does not hold exactly for any non-zero value of k, but it is approximately true for values of k close to 1. We choose k to minimize the variation of $F(\phi;1)$ on $[0,\pi/2]$, and we show in the Appendix that this gives $k\approx 0.988$, and reduces the variation to about 1.4%. The form of $F(\phi;\rho)$ with this value of k is plotted in Fig. 2 for a range of values of ρ^p. The parameter p remains undetermined, and reflects the sensitivity of the microfilament network to changes in the stress field.

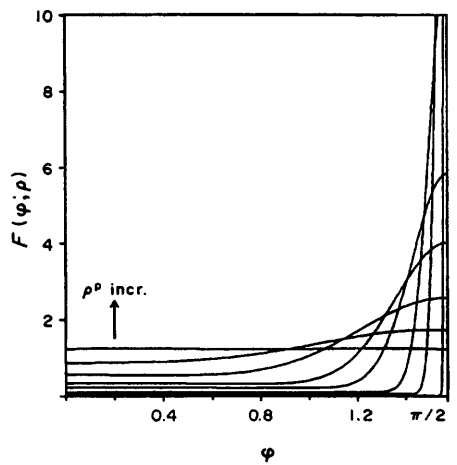

Figure 2. The form of $F(\phi;\rho)$, defined in (1), plotted as a function of ϕ, for $\rho^p=0.01$, 0.05, 0.1, 0.2, 0.3, 0.5, 0.75, 1.0; $F(0;\rho)$ increases with ρ^p. It is sufficient to consider $\rho\leqslant 1$, since $F(\phi;1/\rho)=F(\pi/2-\phi;\rho)$.

We denote by $G_0(\underline{r})$ the total actin filament density at position $\underline{r}$. We assume that each actin filament generates/supports a force along its length; thus the stress exerted by the mesh of actin filaments is determined by the "actin filament density components" along the principal axes of the stress tensor, which are related to F as follows:

$$G_1(\underline{r}) = G_0(\underline{r}) \int_0^{\pi/2} F(\phi; \rho(\underline{r}))\cos\phi \, d\phi$$

$$G_2(\underline{r}) = G_0(\underline{r}) \int_0^{\pi/2} F(\phi; \rho(\underline{r}))\sin\phi \, d\phi = G_0(\underline{r}) \int_0^{\pi/2} F(\phi; 1/\rho(\underline{r}))\cos\phi \, d\phi$$

using the symmetry condition (d). Note that G_1 and G_2 do not depend on the full form of $F(\phi; \rho)$; rather, they depend only on the integral:

$$\int_0^{\pi/2} F(\phi; \rho)\cos\phi \, d\phi \equiv f(\rho), \quad \text{say.} \tag{2}$$

Condition (a) implies that $f(0)=0$ and $f(\infty)=\pi/2$, while condition (b) gives $f(1)=1$. Further, f is a strictly increasing function of ρ^p. Motivated by these properties, we found that to a very good approximation:

$$f(\rho) \approx \frac{(\pi/2)\rho^p}{\rho^p + \pi/2 - 1}$$

as illustrated in Fig. 3. Thus we represent actin filament alignment by the relations:

$$G_1(\underline{r}) = \frac{(\pi/2)\sigma_1^p G_0(\underline{r})}{\sigma_1^p + (\pi/2-1)\sigma_2^p} \tag{3a}$$

$$G_2(\underline{r}) = \frac{(\pi/2)\sigma_2^p G_0(\underline{r})}{\sigma_2^p + (\pi/2-1)\sigma_1^p}. \tag{3b}$$

Under certain conditions, microfilament alignment can occur spontaneously, as a result of the stress exerted by the filaments themselves; more generally, it can be caused by a change in external conditions, for example at the boundary of a cell sheet. We now consider an example of each of these two types of alignment.

3. Applications

3.1. *Auto-alignment of actin filaments.* Actin filament alignment occurs in response to the local stress field, and in the absence of external influences, these stress forces are exerted by the actin filaments themselves. We thus expect intuitively that auto-induction of filament alignment will destabilize a random filament mesh-work if alignment depends sufficiently steeply on stress anisotropy. We now use our model (3) to investigate this phenomenon. Our stability calculation assumes that the two regulatory processes that are reflected in (3) have different time scales. The actin-generated stress alters

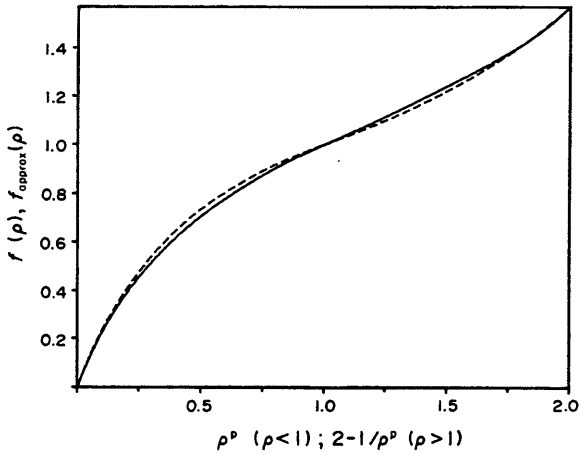

Figure 3. The function $f(\rho)$, defined in (2), compared to $f_{approx}(\rho) \equiv \pi\rho^p/(2\rho^p + \pi - 2)$. For clarity, we plot these functions against ρ^p when $\rho \leqslant 1$ and against $2 - 1/\rho^p$ when $\rho \geqslant 1$. The curves show that f_{approx} provides a good approximation to the transcendental function f.

almost instantaneously with changes in filament density, while the alignment of filaments takes about 10 sec or more to adjust to changes in the stress field (Kolega, 1986; Chen, 1981).

We consider the very simple case of a cell sheet at equilibrium, with its boundaries held fixed and with no strain at any point. The sheet will then be under tension, even though the strain field is zero, because of the traction forces exerted by the cells. This traction stress will depend on the local actin filament density, and following previous authors (for example Oster, 1984; Oster *et al.*, 1985a), we take this dependence to be a simple proportionality. Thus:

$$\sigma_1 = \tau_0 G_1 \quad \text{and} \quad \sigma_2 = \tau_0 G_2 \tag{4}$$

where τ_0 is a positive constant, and the 1- and 2-axes are in this case in arbitrary orthogonal directions. Writing $\gamma = G_1/G_2$, these imply that $\rho = \gamma$. As discussed above, this dependence of stress ρ on changes in alignment γ is essentially instantaneous, while the dependence of γ on changes in ρ that is implied by our equations (3) occurs on a longer time scale. Together, (3) and (4) give an equation for γ, with multiple solutions. We now use the difference in time scale of the two responses to investigate the stability of these various equilibrium configurations of the microfilament network.

Suppose that $\rho = \rho_e$ and $\gamma = \gamma_e$ is a solution of (3) and (4), so that:

$$\gamma_e = \rho_e = \frac{\rho_e^p[1 + (\pi/2 - 1)\rho_e^p]}{\rho_e^p + \pi/2 - 1}.$$

Then our assumption that (4) is satisfied instantaneously implies that if we perturb the alignment ratio to a new value $\gamma_e+\varepsilon$, the stress ratio will simultaneously change to $\rho_e+\varepsilon$. If this value of the stress ratio ρ were maintained, our equations (3) imply that the actin filament density ratio would move to the value:

$$\gamma_{\text{pert}}=\frac{(\rho_e+\varepsilon)^p[1+(\pi/2-1)(\rho_e+\varepsilon)^p]}{(\rho_e+\varepsilon)^p+\pi/2-1}.$$

The initial direction of change of alignment ratio γ is thus increasing if $\gamma_{\text{pert}}>\gamma_e+\varepsilon$; and since ρ follows γ instantaneously, this entails an increase of ρ also, that is an increase in the departure from equilibrium—in other words, an instability. Thus (ρ_e, γ_e) will be stable to small perturbations if and only if:

$$\frac{d}{d\rho}\left\{\frac{\rho^p[1+(\pi/2-1)\rho^p]}{\rho^p+\pi/2-1}\right\}_{\rho=\rho_e}<1$$

since this derivative is clearly non-negative for all ρ. We now write

$$H(\rho)\equiv\frac{\rho^p[1+(\pi/2-1)\rho^p]}{\rho^p+\pi/2-1}-\rho. \tag{5}$$

Then for a solution of our model we require $H(\rho)=0$, and this solution is stable if and only if $H'(\rho)<0$. In Fig. 4 we plot $H(\rho)$ for a number of values of p. We restrict attention to $0\leqslant\rho\leqslant1$, since our problem is symmetric in the 1- and 2-axes. There is an abrupt change in the form of H as p increases through 1, since:

$$H'(0)=\begin{cases}\infty & \text{for } 0<p<1\\ (4-\pi)/(\pi-2) & \text{for } p=1\\ -1 & \text{for } p>1.\end{cases}$$

The figure shows that the number of solutions and their stability depends on p:

for $0<p\leqslant1$: $\rho=0$ is an unstable solution
$\rho=1$ is a stable solution

for $1<p<p_{\text{crit}}$: $\rho=0$ and $\rho=1$ are both stable solutions
There is also an unstable solution $\rho=\hat{\rho}\in(0, 1)$

for $p>p_{\text{crit}}$: $\rho=0$ is a stable solution
$\rho=1$ is an unstable solution.

Here p_{crit} is defined by $H'(1)=0$, which gives $p_{\text{crit}}=\frac{1}{2}[1+1/(\pi/2-1)]\approx1.38$. In the case $1<p<p_{\text{crit}}$, the two stable solutions $\rho=0$ and $\rho=1$ have basins of

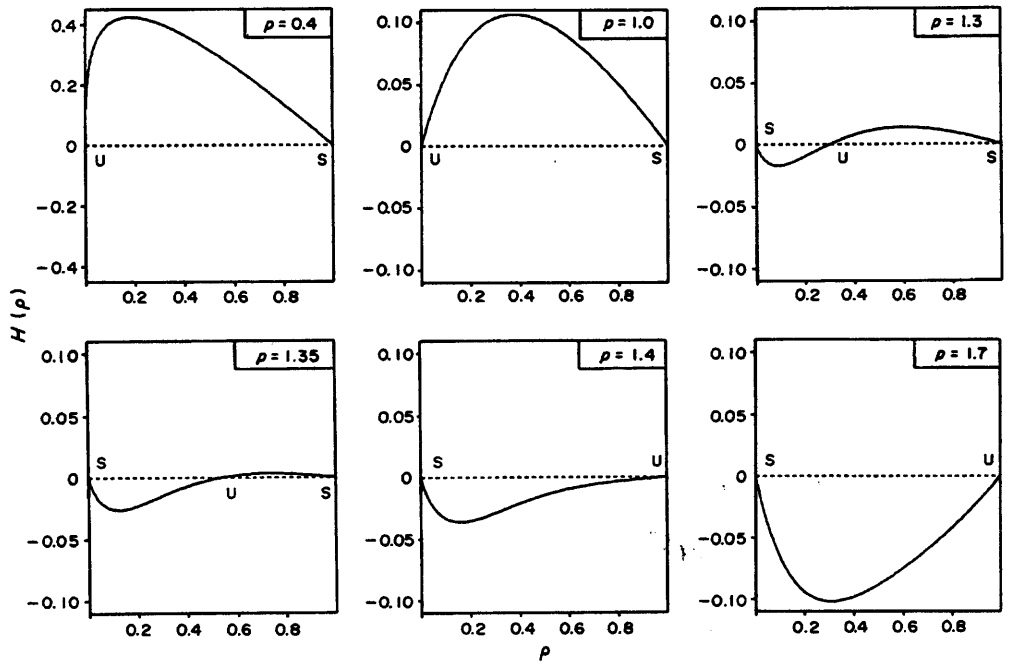

Figure 4. The function $H(\rho)$, defined in (5), for a range of values of the parameter p, which reflects the sensitivity of the microfilament network to changes in the stress field. We restrict attention to $0 \leqslant \rho \leqslant 1$, since our problem is symmetric in the 1- and 2-axes. Equilibrium configurations of the microfilament network satisfy $H(\rho)=0$, and are stable if and only if $H'(\rho)<0$. In the figure, we denote stable and unstable equilibria by S and U, respectively.

attraction $[0, \hat{\rho})$ and $(\hat{\rho}, 1]$, and as shown in Fig. 5, $\hat{\rho}$ is extremely small for values of p as high as 1.1, so that for practical purposes $\rho=0$ is then unstable.

Recalling that $\rho=\gamma=G_1/G_2$ at equilibrium, $\rho=0$ corresponds to unidirectional actin filaments, while $\rho=1$ corresponds to a random filament meshwork. Thus our model predicts that the configuration of the microfilament network in a cell sheet at rest will depend on the sensitivity of actin filament alignment to changes in the stress field. When this sensitivity is low, the network will have a random, mesh-like arrangement, but when it is sufficiently high, this random configuration will be driven unstable, and all the microfilaments will become spontaneously aligned in a single, random direction. Such spontaneous filament alignment could play an important role in morphogenetic processes such as convergent extension (Gerhart and Keller, 1986; Lewis *et al.*, in preparation).

3.2. *Boundary-induced filament alignment.* Stress-induced alignment of actin will also have important effects in the responses of an epithelial sheet to externally applied forces and boundary conditions. This is well exemplified in

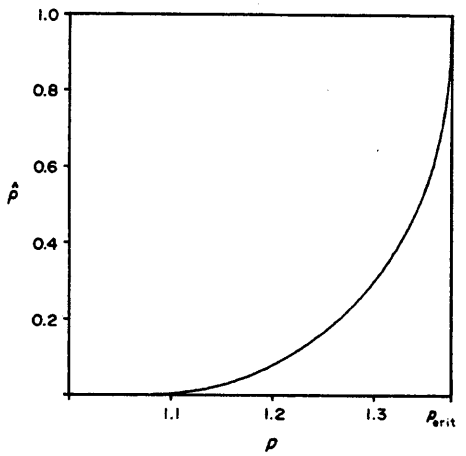

Figure 5. The value of the unstable solution $\hat{\rho} \in (0, 1)$ of $H(\rho) = 0$. This solution exists for $1 < p < p_{crit}$, but is very small when p is close to 1, so that the anisotropic solution $\rho = 0$ of $H(\rho) = 0$ has a very small basin of attraction.

the case of wound healing, where a surgical cut creates an epidermal free edge, and the cellular response to wounding is to a large extent a response to this free edge. In the epidermis of chick and mouse embryos, Martin and Lewis (1991, 1992) have recently shown that wounding induces marked alignment of actin filaments, resulting in a thick cable of filamentous actin around almost all of the wound margin, localized within the leading row of basal cells. By contrast, wounding in adult epithelia induces increased proliferation and lamellipodial crawling (Winter, 1962, 1972; Clark, 1989; Sherratt and Murray, 1990, 1991, 1992). We now use our model (3) to investigate the initial formation of this actin cable, as an example *in vivo* microfilament alignment caused by a free boundary. In the epidermal cell sheet, the intracellular actin filaments are linked via cell–cell adherens junctions in a transcellular network, and following wounding this network undergoes rapid changes, forming a new quasi-equilibrium state in which an actin cable runs around the wound margin; this cable appears to act like a purse-string, causing the wound gradually to close. Here we restrict attention to the quasi-equilibrium configuration, with its prominent feature of an actin cable at the wound margin.

We take the microfilament network as two-dimensional, since its thickness is much smaller than the typical wound dimensions of about 500 μm, and for simplicity, we consider the case of a circular wound. The principal axes of the stress tensor $\underline{\underline{\sigma}}$ will then be aligned at all points with the radial and tangential coordinate axes. In addition to the traction stress, we also have to take account of strain and elastic contributions to the stress, since the epithelium is displaced. At equilibrium, there will be no viscous contribution to $\underline{\underline{\sigma}}$, and we take its principal values to be given by:

$$\sigma_{rr} = \underbrace{G_r[E\varepsilon_{rr} + \Gamma\nabla\cdot\underline{u}]}_{\text{elastic stress}} + \underbrace{G_r\tau}_{\text{active contraction stress}} \quad (6a)$$

$$\sigma_{\theta\theta} = \underbrace{G_\theta[E\varepsilon_{\theta\theta} + \Gamma\nabla\cdot\underline{u}]}_{\text{elastic stress}} + \underbrace{G_\theta\tau}_{\text{active contraction stress}}. \quad (6b)$$

Here $G_r(\underline{r})$ and $G_\theta(\underline{r})$ are the radial and tangential "components" of actin filament density at the material point initially at $\underline{r}$, $\underline{u}(\underline{r})$ is the displacement of that point from its pre-wounding position, ε_{rr} and $\varepsilon_{\theta\theta}$ are the principal values of the strain tensor $\underline{\underline{\varepsilon}} = \frac{1}{2}(\nabla\underline{u} + \nabla\underline{u}^T)$, τ is the traction stress per actin filament, and E and Γ are positive constants. The form (6) is the standard representation of stress at equilibrium in the Oster–Murray approach (see in particular the model of Murray and Oster, 1984a, for epithelial morphogenesis), although in previous applications, $G_r \equiv G_\theta$. Many authors have taken the traction stress per actin filament, τ, to be an increasing function of the local compaction, since as the microfilament network is compressed, the degree of filament overlap increases and additional myosin cross-bridges form (Oster, 1984; Oster and Odell, 1984a,b; Oster *et al.*, 1985a). For generality, we therefore take $\tau = \tau_0/(1-\beta\Omega)$, where $\tau_0 > 0$ and $\beta \geqslant 0$ are constants, and Ω is the fraction of its pre-wounding area by which a small region of cytogel contracts in response to wounding. In a radially symmetric circular geometry, $\Omega = 1-(1+u')(1+u/r)$, where $r = |\underline{r}|$, $\underline{u}(\underline{r}) = u(r)\hat{\underline{r}}$, and prime denotes d/d$r$.

The models (3) and (6) together give implicit equations for stress as a function of strain:

$$\sigma_{rr} = \frac{(\pi/2)\sigma_{rr}^p G_0}{\sigma_{rr}^p + (\pi/2-1)\sigma_{\theta\theta}^p}\cdot\{Eu' + \Gamma(u'+u/r) + \tau_0/[1+\beta(u'+u/r+uu'/r)]\} \quad (7a)$$

$$\sigma_{\theta\theta} = \frac{(\pi/2)\sigma_{\theta\theta}^p G_0}{\sigma_{\theta\theta}^p + (\pi/2-1)\sigma_{rr}^p}\cdot\{Eu/r + \Gamma(u'+u/r) + \tau_0/[1+\beta(u'+u/r+uu'/r)]\}. \quad (7b)$$

At equilibrium, these elastic and traction stresses balance the elastic restoring forces due to attachment to the substratum. Following Murray and Oster (1984a), we represent the restoring forces by $\lambda G_0\underline{u}$, where the positive constant λ reflects the strength of the attachments. The dependence on G_0 arises because we assume that the attachments are fixed in the basal lamina and that this becomes wrinkled (so that the attachments are compressed) in response to wounding, to an extent reflecting the compaction of the cell sheet. Experimental justification for this dependence is given by Hergott *et al.* (1989), who find that the density of focal contacts increases in parallel to that of actin filament bundles in the response of chick embryonic corneal cells to wounding in an organ culture system.

Thus the equation to be solved for the new equilibrium configuration is:

$$\nabla \cdot \underline{\underline{\sigma}} = \lambda G_0 \underline{u} \tag{8}$$

with $\underline{\underline{\sigma}}$ given by (7). For general values of p, (7) cannot be solved analytically to give expressions for σ_{rr} and $\sigma_{\theta\theta}$ as functions of u. We therefore restrict attention to the case $p=1$. We have shown in the previous section that there will then be no spontaneous microfilament alignment prior to wounding. Therefore, solutions of (7) in which one of the principal values of stress is identically zero are not relevant, since we require both G_r and G_θ to be non-zero at points far from the wound. The solutions for σ_{rr} and $\sigma_{\theta\theta}$ in the case $p=1$ are thus:

$$\sigma_{rr} = G_0 \left\{ \frac{E(2u' - (\pi-2)u/r)}{4-\pi} + \Gamma(u' + u/r) + \frac{\tau_0}{1+\beta(u'+u/r+uu'/r)} \right\} \tag{9a}$$

$$\sigma_{\theta\theta} = G_0 \left\{ \frac{E(2u/r - (\pi-2)u')}{4-\pi} + \Gamma(u' + u/r) + \frac{\tau_0}{1+\beta(u'+u/r+uu'/r)} \right\}. \tag{9b}$$

It remains to consider the relationship between G_0 and $\underline{u}$. The results we present here are based on the assumption that the total amount of filamentous actin within each cell remains constant during the initial response to wounding. Since we are treating the cell sheet as a continuum, the mathematical formulation of this assumption is $G_0(1-\Omega)=\kappa$, a spatially homogeneous constant; recall that $\Omega = 1-(1+u')(1+u/r)$ is the local compaction. The implications of assuming more localized conservation of filamentous actin are presented elsewhere (Sherratt, 1992). To clarify the roles of the various model parameters, we nondimensionalize (8) by defining:

$$r^* = r/R \qquad u^* = u/R \qquad E^* = E/\tau_0 \qquad \Gamma^* = \Gamma/\tau_0 \qquad \lambda^* = \lambda R^2/\tau_0$$

where * denotes a dimensionless quantity, and R is the initial wound radius. Substituting these rescalings into (8) and (9), and dropping the asterisks for notational simplicity, gives a highly nonlinear second order ordinary differential equation for $u(r)$:

$$u'' = \frac{1}{[2E/(4-\pi)+\Psi](r+u)+\Gamma(r-u^2/r)} \cdot \left\{ \lambda r u \left[1 + u' + \frac{u}{r} + \frac{uu'}{r} \right] - \left(u' - \frac{u}{r} \right) \left[\frac{2E}{4-\pi} \left(1 + \frac{u}{r} - u'^2 + \frac{uu'}{r} \right) + \Gamma(1-u'^2) + \Psi(1+u') \right] \right\} \tag{10}$$

where

$$\Psi = \frac{(\pi-2)Eu}{(4-\pi)r} - \frac{1+\beta+2\beta(u'+u/r+uu'/r)}{[1+\beta(u'+u/r+uu'/r)]^2}.$$

We treat the cell sheet as infinite, which is valid provided the wound area is small compared to the whole sheet. The biologically appropriate boundary conditions are then $\sigma_{rr}=0$ at $r=1$ (the wound edge) and $u=0$ at $r=\infty$.

Within the context of our continuum approximation across the cell sheet, the actin cable observed experimentally should correspond to a sharp increase in the calculated density of tangentially aligned actin filaments near the wound edge. This indeed is our finding in the model solutions for a wide range of parameter values: a typical solution is shown in Fig. 6. Here we plot G_r and G_θ as functions of r; (2.3) and (3.9) together imply that:

$$G_r = G_0 \frac{\Gamma(u'+u/r)+1/[1-\beta\Omega]+E[2u'-(\pi-2)u/r]/(4-\pi)}{\Gamma(u'+u/r)+1/[1-\beta\Omega]+Eu'} \tag{11a}$$

$$G_\theta = G_0 \frac{\Gamma(u'+u/r)+1/[1-\beta\Omega]+E[2u/r-(\pi-2)u']/(4-\pi)}{\Gamma(u'+u/r)+1/[1-\beta\Omega]+Eu/r}. \tag{11b}$$

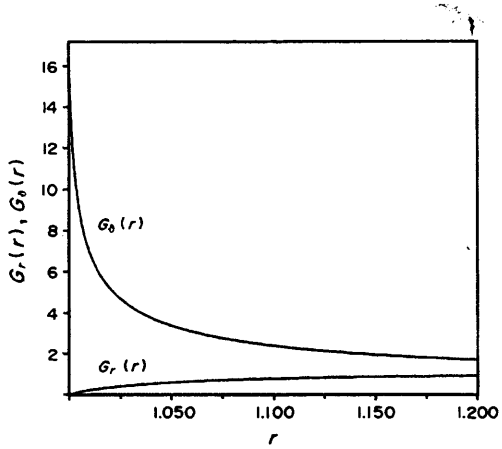

Figure 6. The effective densities of radially and tangentially aligned actin filaments, G_r and G_θ, defined in (11). The solution for $u(r)$ is obtained by solving the model equation (10) numerically using a finite difference scheme and Newton's method, with deferred correction and continuation in β (Pereyra, 1979). The dimensionless parameter values are $E=0.5, \Gamma=0.8, \lambda=3, \beta=0.485$. This solution exhibits a sharp increase in the density of tangentially aligned actin near the wound edge, and thus reflects the phenomenon of the actin cable found experimentally by Martin and Lewis (1991, 1992).

The corresponding model without filament alignment can be obtained by setting the parameter $p=0$ (recall that the above solutions are for $p=1$). We anticipate that the absence of stress-induced alignment of microfilaments parallel to the wound edge will increase the radial traction stress exerted by aggregated actin near this edge, and thus reduce the ability of the restraining elastic stress to hold the epidermal sheet in mechanical equilibrium. This is

confirmed by the model solutions: for the parameter values used in Fig. 6, a solution of the model does not exist in the case $p=0$ (Sherratt, 1992). Model solutions do exist in this case for larger values of the elasticity parameters E and Γ, although the parameter domain in which a solution exists is considerably smaller than in the case $p=1$. Moreover, for appropriate parameters, these solutions do imply an aggregation of actin density G_0 near the wound edge; however, they are unable to capture the experimentally observed tangential alignment of this aggregated actin.

Biologically, our results suggest that the initial formation of the actin cable at the edge of embryonic epidermal wounds can be explained simply as a by-product of the post-wounding mechanical equilibrium in the epidermis, without ascribing any special properties, such as elevated levels of regulatory chemical or a phenotype change, to the cells at the wound edge. Such changes may occur (Pender and McCulloch, 1991), but our model suggests that they are not necessary for the formation of an actin cable.

4. Conclusions. Despite considerable biological evidence for stress-induced alignment of the cellular microfilament network, the phenomenon has been neglected in previous mechanical models for tissue deformation. We have developed a model for this effect, in which actin filaments align according to the local anisotropy of the stress field, and our formulation includes a parameter reflecting the sensitivity of this response. We have used the model to investigate the equilibrium state of the microfilament network in a cell sheet at rest, and the response of embryonic epidermis to wounding. In the former system, filament alignment can occur spontaneously, while in the latter it is induced by the free edge at the wound front. These applications suggest that stress-induced actin filament alignment could play a key role in some biological systems.

We would like to thank Professor J. D. Murray (Dept of Applied Mathematics, University of Washington) and Dr Paul Martin (Dept of Human Anatomy, University of Oxford) for their help with various aspects of this work. J.A.S. was in part supported by a graduate studentship from the Science and Engineering Research Council of Great Britain, and in part by a Junior Research Fellowship at Merton College, Oxford.

APPENDIX

The value of k. The definition (1) of $F(\phi;\rho)$ does not exactly satisfy condition (c), that $F(\phi;1)$ is constant. In this Appendix, we show that the condition can be satisfied to a good approximation for appropriate values of k. Specifically, we look for the value of k, not near zero, that minimizes the variation of:

$$g(\phi)=\exp[-k\phi^2]+\exp[-k(\pi/2-\phi)^2]\equiv F(\phi;1)/F_0(1) \tag{A1}$$

on $0 \leqslant \phi \leqslant \pi/2$. [Trivially, $g(\phi) \equiv 2$ when $k = 0$, but this case is not biologically relevant.] The form of $g(\phi)$ for a selection of values of k is shown in Fig. A1. Differentiating equation (A1) with respect to ϕ gives:

$$\frac{dg}{d\phi} = 2ke^{-k\phi^2}(\pi/2-\phi)\left[\exp\{k\pi(\phi-\pi/4)\} - \frac{\phi}{\pi/2-\phi}\right]$$

$$= 0 \Leftrightarrow \exp\{k\pi(\phi-\pi/4)\} = \frac{\phi}{\pi/2-\phi}. \tag{A2}$$

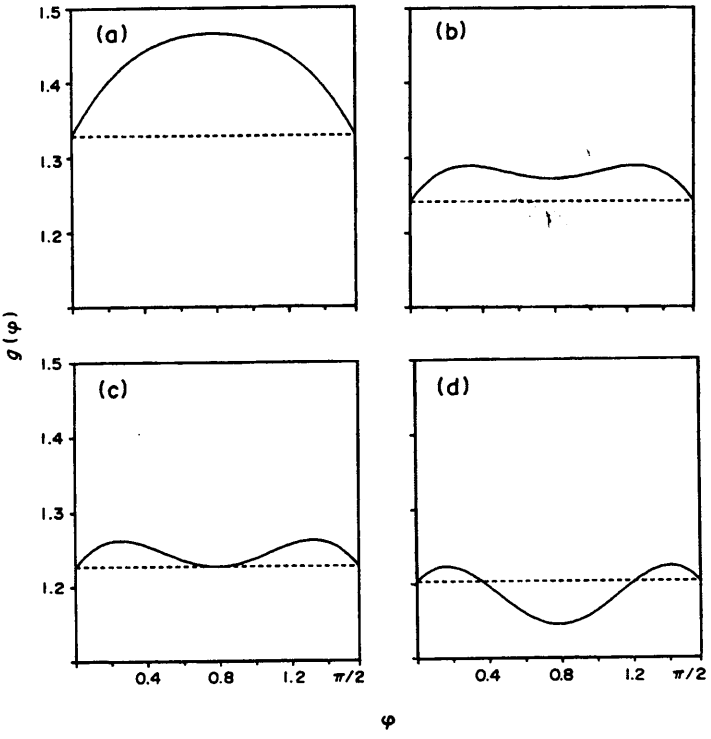

Figure A1. The form of the function $g(\phi)$, defined in equation (A1), as the parameter k varies. (a) $k = 0.7$; (b) $k = 0.93$; (c) $k = k_{crit2} \approx 0.988$, defined in (A3); (d) $k = 1.1$. The dashed line indicates the equal values of $g(0)$ and $g(\pi/2)$.

It is sufficient to consider this equation on $[0, \pi/4]$, by the symmetry of $g(\phi)$ about $\phi = \pi/4$. The two sides of (A2) are plotted in Fig. A2 for a range of values of k. From this, it is clear that in addition to the root at $\phi = \pi/4$, equation (A2) has a second root in $(0, \pi/4)$ if $k > k_{crit1}$, where k_{crit1} satisfies:

$$\frac{d}{d\phi}\left[\exp\{k\pi(\phi-\pi/4)\} - \frac{\phi}{\pi/2-\phi}\right]\Bigg|_{\phi=\pi/4} = 0.$$

This uniquely determines k_{crit1} as $8/\pi^2$, ≈ 0.81.

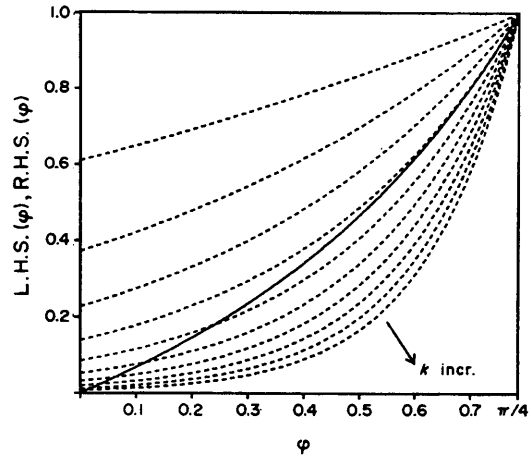

Figure A2. The right-hand (full curve) and left-hand (dashed curves) sides of equation (A2) for $k=0.2, 0.4, 0.6, \ldots, 2.0$; the value of the left-hand side decreases, for any given ϕ, as k increases. The number of solutions of the equation on $[0, \pi/4]$ increases from one to two as k increases through the critical value k_{crit1}.

We now write:

$$g_{max}(k) = \max_{0 \leq \phi \leq \pi/2} g(\phi) \quad \text{and} \quad g_{min}(k) = \min_{0 \leq \phi \leq \pi/2} g(\phi).$$

By symmetry these are also the maximum and minimum values, respectively, on $[0, \pi/4]$. Then for $k < k_{crit1}$:

$$g_{max}(k) = g(\pi/4) = 2e^{-k\pi^2/16}$$

$$\text{and} \quad g_{min}(k) = g(0) = 1 + e^{-k\pi^2/4}.$$

For $k > k_{crit1}$, $g_{max}(k) = g(\phi_{max})$, where ϕ_{max} is the unique solution of:

$$\exp\{k\pi(\phi - \pi/4)\} = \frac{\phi}{\pi/2 - \phi}$$

in the open interval $(0, \pi/4)$. This cannot be found analytically, but can easily be calculated numerically for a given value of k. Also for $k > k_{crit1}$, $g_{min}(k) = \min\{g(0), g(\pi/4)\}$. It is clear from Fig. A1 that there is a critical value k_{crit2} such that:

for $k_{crit1} < k < k_{crit2}$, $g(0) < g(\pi/4)$, so that $g_{min}(k) = 1 + e^{-k\pi^2/4}$

and for $k > k_{crit2}$, $g(0) > g(\pi/4)$, so that $g_{min}(k) = 2e^{-k\pi^2/16}$.

Here k_{crit2} satisfies $g(0) = g(\pi/4)$, that is:

$$1 + e^{-k\pi^2/4} = 2e^{-k\pi^2/16}.$$

Thus $k_{crit2} = -(16/\pi^2)\log x$, where x is a solution of $x^4 - 2x + 1 = 0$. Now:

$$x^4 - 2x + 1 = (x-1)(x^3 + x^2 + x - 1).$$

The root $x=1$ corresponds to the trivial case of $g(\phi)\equiv 2$ when $k=0$. Substituting $x=\frac{1}{3}(2\sqrt{2}\sinh\hat{x}-1)$ in the cubic equation shows that this has a unique solution, which gives:

$$k_{crit2}=-\frac{16}{\pi^2}\log\left\{\frac{2\sqrt{2}}{3}\sinh\left[\frac{1}{3}\sinh^{-1}\left(\frac{17}{2\sqrt{2}}\right)\right]-\frac{1}{3}\right\}\approx 0.987886. \tag{A3}$$

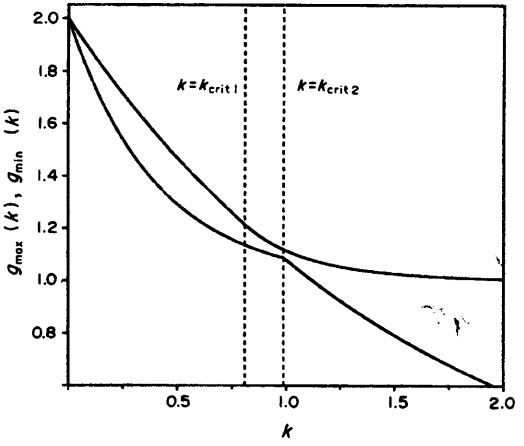

Figure A3. The maximum and minimum values of $g(\phi)$ on $[0, \pi/2]$, $g_{max}(k)$ and $g_{min}(k)$, plotted as functions of the parameter k. The vertical lines $k=k_{crit1}$ and $k=k_{crit2}$ are also drawn. Trivially, $g(\phi)\equiv 2$ when $k=0$, but for values of k away from zero, the variation of $g(\phi)$ is minimized in both an absolute and relative sense when $k=k_{crit2}$.

In Fig. A3 we plot $g_{max}(k)$ and $g_{min}(k)$ as functions of k. These suggest that the variation of $g(\phi)$ is minimized when $k=k_{crit2}$, and this is confirmed by numerical minimization using quadratic interpolation. Specifically, numerical calculations show that both $[g_{max}(k)-g_{min}(k)]$ and $[g_{max}(k)-g_{min}(k)]/[g_{max}(k)+g_{min}(k)]$ are minimized at $k=k_{crit2}$, for k not near zero. [Trivially, $g_{max}(k)=g_{min}(k)$ when $k=0$, since then $g(\phi)\equiv 2$.] Thus the variation of $g(\phi)$ on $0\leqslant\phi\leqslant\pi/2$ is minimized in both an absolute and relative sense when $k=k_{crit2}$. For this value of k, the variation of g on $[0, \pi/2]$ is about 1.4%.

LITERATURE

Chen, W. 1981. Mechanism of retraction of the trailing edge during fibroblast movement. *J. Cell Biol.* **90**, 187–200.

Clark, R. A. F. 1989. Wound repair. *Curr. Op. Cell Biol.* **1**, 1000–1008.

Franke, R. P., M. Grafe, H. Schnittler, D. Seiffge, C. Mittermayer and D. Drenckhahn. 1984. Induction of human vascular endothelial stress fibres by fluid shear stress. *Nature* **307**, 648–649.

Gerhart, J. and R. Keller. 1986. Region-specific cell activities in amphibian gastrulation. *Ann. Rev. Cell Biol.* **2**, 201–229.

Harris, A. K. 1982. Traction and its relations to contraction in tissue cell locomotion. In *Cell*

Behaviour, R. Bellairs, A. Curtis and G. Dunn (Eds), pp. 109–134. Cambridge: Cambridge University Press.

Hergott, G. J., M. Sandig and V. I. Kalnins. 1989. Cytoskeletal organisation of migrating retinal pigment epithelial cells during wound healing in organ culture. *Cell Motil.* **13**, 83–93.

Kolega, J. 1986. Effects of mechanical tension on protrusive activity and microfilament and intermediate filament organization in an epidermal epithelium moving in culture. *J. Cell Biol.* **102**, 1400–1411.

Ludueña, M. A. and N. K. Wessells. 1973. Cell locomotion, nerve elongation and microfilaments. *Dev. Biol.* **30**, 427–440.

Martin, P. and J. Lewis. 1991. The mechanics of embryonic skin wound healing—limb bud lesions in mouse and chick embryos. In *Fetal Wound Healing: a Paradigm of Tissue Repair*, N. S. Adzick and M. T. Longaker (Eds), pp. 265–279. New York: Elsevier.

Martin, P. and J. Lewis. 1992. Embryonic wound healing: actin cables and epidermal movement. Submitted.

Murray, J. D., G. F. Oster and A. K. Harris. 1983. A mechanical model for mesenchymal morphogenesis. *J. math. Biol.* **17**, 125–129.

Murray, J. D. and G. F. Oster. 1984a. Generation of biological pattern and form. *IMA J. Math. appl. med. Biol.* **1**, 51–75.

Murray, J. D. and G. F. Oster. 1984b. Cell traction models for generating pattern and form in morphogenesis. *J. math. Biol.* **19**, 265–279.

Murray, J. D., P. K. Maini and R. T. Tranquillo. 1988. Mechanochemical models for generating biological pattern and form in development. *Phys. Rep.* **171**, 59–84.

Odell, G. M., G. Oster, P. Alberch and B. Burnside. 1981. The mechanical basis of morphogenesis. *Dev. Biol.* **85**, 446–462.

Oster, G. F. 1984. On the crawling of cells. *J. Embryol. exp. Morphol.* **83** Suppl., 329–364.

Oster, G. F. and G. M. Odell. 1984a. Mechanics of cytogels I: oscillations in *Physarum*. *Cell Motil.* **4**, 469–503.

Oster, G. F. and G. M. Odell. 1984b. The mechanochemistry of cytogels. *Physica* **D12**, 333–350.

Oster, G. F., J. D. Murray and A. K. Harris. 1983. Mechanical aspects of mesenchymal morphogenesis. *J. Embryol. exp. Morphol.* **78**, 83–125.

Oster, G. F., J. D. Murray and G. M. Odell. 1985a. The formation of microvilli. In *Molecular Determinants of Animal Form*, G. M. Edelman (Ed.), pp. 365–384. New York: Alan R. Liss.

Oster, G. F., J. D. Murray and P. K. Maini. 1985b. A model for chondrogenic condensations in the developing limb: the role of extracellular matrix and cell tractions. *J. Embryol. exp. Morphol.* **89**, 93–112.

Pender, N. and C. A. G. McCulloch. 1991. Quantitation of actin polymerization in two human fibroblast sub-types responding to mechanical stretching. *J. Cell Sci.* **100**, 187–193.

Pereyra, V. 1979. PASAVA3: an adaptive finite-difference program for first order nonlinear ordinary boundary problems. In *Codes for Boundary Value Problems in Ordinary Differential Equations*. B. Childs, M. Scott, J. W. Daniel, E. Denman and P. Nelson (Eds), *Lecture Notes in Computer Science*, Vol. 76, pp. 67–88.

Pollard, T. D. 1990. Actin. *Curr. Op. Cell Biol.* **2**, 33–40.

Sherratt, J. A. 1992. Actin aggregation and embryonic epidermal wound healing. *J. math. Biol.*, in press.

Sherratt, J. A. and J. D. Murray. 1990. Models of epidermal wound healing. *Proc. r. Soc. Lond.* **B241**, 29–36.

Sherratt, J. A. and J. D. Murray. 1991. Mathematical analysis of a basic model for epidermal wound healing. *J. math. Biol.* **29**, 389–404.

Sherratt, J. A. and J. D. Murray. 1992. Epidermal wound healing: a theoretical approach. *Comm. theor. Biol.*, in press.

Spooner, B. S., K. M. Yamada and N. K. Wessells. 1971. Microfilaments and cell locomotion. *J. Cell Biol.* **49**, 595–613.

Stopak, D., N. K. Wessells and A. K. Harris. 1985. Morphogenetic rearrangement of injected collagen in developing chicken limb buds. *Proc. natn. Acad. Sci. U.S.A.* **82**, 2804–2808.

Valberg, P. A. and D. F. Albertini. 1985. Cytoplasmic motions, rheology, and structure probed by a novel magnetic particle method. *J. Cell Biol.* **101**, 130–140.

Wechezak, A. R., T. N. Wight, R. F. Viggers and L. R. Sauvage. 1989. Endothelial adherence under shear stress is dependent upon microfilament reorganisation. *J. cell. Physiol.* **139**, 136–146.

Winter, G. D. 1962. Formation of the scab and the rate of epithelialization of superficial wounds in the skin of the young domestic pig. *Nature* **193**, 293–294.

Winter, G. D. 1972. Epidermal regeneration studied in the domestic pig. In *Epidermal Wound Healing*, H. I. Maibach and D. T. Rovee (Eds), pp. 71–112. Chicago: Year Book Med. Publ.

Received 19 December 1991
Revised 24 April 1992